GEOPHYSICAL RESEARCH LETTERS, VOL. 25, NO. 3, PAGES 405-408, February 1, 1998

Observations of high–frequency scattered energy associated with the core phase *PKKP*

Paul S. Earle,[1] Peter M. Shearer

Cecil H. and Ida M. Green Institute of Geophysics and Planetary Physics, Scripps Institution of Oceanography, University of California, San Diego, La Jolla.

Abstract. Stacks of global seismic network data reveal emergent high–frequency (∼1 Hz) energy extending back from the *PKKP c* caustic at 72° to a distance of about 60°. The arrival's emergent onset, long duration (∼150 s), apparent slowness, and proximity to the core phase $PKKP$ indicate a deep scattering origin. However, the amplitude and timing of the observations are difficult to explain with simple models of $PKKP$ scattering.

Introduction

Seismograms from distant earthquakes contain body–wave arrivals resulting from a variety of interactions with subsurface structure, including refractions, diffractions, reflections, phase conversions, and scattering. Analysis of these signals over a broad frequency range reveals details of Earth structure at length scales from tens to thousands of kilometers (see *Lay and Wallace*, 1995 for background).

Fine–scale deep Earth structure can be examined by studying high–frequency (∼1 Hz) waveforms and scattered energy. The limited pulse distortion of short–period core reflected phases places upper bounds of 500 m on CMB topography over horizontal scale lengths of 50 to 200 km [*Vidale and Benz*, 1992]. The onset time of scattered energy arriving before the core phase $PKPdf$ requires the presence of small–scale (∼10 km) velocity heterogeneity near the base of the mantle [e.g., *Cleary and Haddon*, 1972], with more recent analysis [*Hedlin et al.*, 1997] indicating that these features exist throughout the mantle. The extended uniformly polarized coda of high–frequency P_{diff} arriving beyond the core shadow is consistent with multiple scattering in a low–velocity zone near the CMB [*Bataille and Lund*, 1996].

A large number of both major and minor seismic phases have been identified, and in most cases it is understood which structures contribute to the observations. Here we document an extended wavetrain of high–frequency energy apparently associated with the core phase $PKKP$. The character of the arrivals suggests they originate as deep scattering from the mantle or core, but so far we have been unable to identify a specific mechanism that can explain the observations.

$PKKP$ observations

The predicted travel–time curve for $PKKP$ is shown in Figure 1, together with example ray paths for the different branches. All branches of $PKKP$ reflect once from the underside of the CMB but turn at different depths within the Earth. $PKKP$ is most readily detected in vertical–component, high–frequency seismic records (long–period records are contaminated by surface wave arrivals). Typically only the *ab* and *bc* branches of $PKKP$ are observed [e.g., *Astiz et al.*, 1996]; the *df* leg is very weak due to the effect of inner–core attenuation and the small CMB reflection coefficient at near–vertical incidence angles. In addition to the direct $PKKP$ arrivals, observations have been made of scattered $PKKP$ energy that provide further insight into Earth structure. Detection of scattered $PKKPab$ and $PKKPbc$ energy beyond 125° supports the existence of small–scale heterogeneities at the base of the mantle [*Doornbos*, 1974]. $PKKP$ precursors in the distance range 80° to 120° have been used to place upper bounds (order 100 m) on small–scale (∼10 km) CMB topography [*Doornbos*, 1980; *Earle and Shearer*, 1997]. Isolated array observations of seismic arrivals near 60° with $PKKPdf$ travel times and $PKKPbc$ slownesses, interpreted as energy scattered at the CMB [*Chang and Cleary*, 1978], have been a source of controversy [*Doornbos*, 1980].

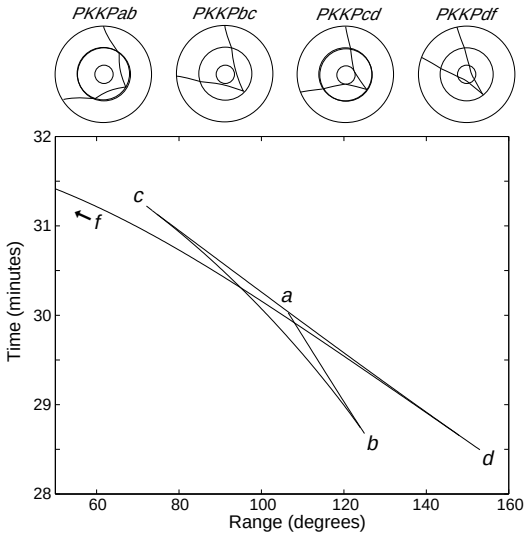

Figure 1. Example ray paths for the *ab, bc, cd, and df* branches of $PKKP$ and travel–time curves computed from the *iasp*91 velocity model. The different branches of $PKKP$ are labeled in lowercase italics and ranges are given as source–receiver separation. $PKKP$ is a "wrap around" phase, meaning the energy travels distances greater than 180°; a $PKKP$ arrival recorded at a source–receiver separation of 80° has traveled 280°.

[1]Now at Department of Earth and Space Sciences, University of California, Los Angeles.

Paper number 97GL53365.
0094-8534/98/97GL-53365$0500

Data selection and stacking

We apply an envelope function stacking technique to image the character of high–frequency energy arriving in the vicinity of $PKKP$. We recently used a similar method to study $PKKP$ precursors between 80° and 120° [*Earle and Shearer*, 1997]. The stacking technique requires the use of a reference phase to normalize the amplitudes. To extend our results to ranges as short as 55° (where direct $PKKP$ cannot be seen), we use $P'P'$ as the reference phase because it is observed over the desired distance range and travels a similar path to $PKKP$ ($P'P'$ reflects from the underside of Earth's surface rather than the CMB, thus $P'P'$ contains two more mantle legs than $PKKP$).

We select high quality observations of $P'P'$ from the 22,231 broadband vertical–component seismograms stored in the IRIS FARM archive over the distance range 55° to 88° from earthquakes occurring between 1988 through 1995. After initial filtering and decimation to 5 samples per second, the high–gain recordings contain frequencies from below 0.01 Hz to 2.5 Hz. To eliminate signal–generated and ambient noise at low frequencies, the data are filtered to a narrow high–frequency band (0.4 to 2.5 Hz).

After filtering, we select an initial set of seismograms with good signal–to–noise (STN) for stacking. We define the STN as the ratio of the maximum value in a 45 s signal window starting 5 s before $P'P'$ to that in a 130 s noise window beginning 200 s before $P'P'$. At distance ranges less than the $P'P'$ *b* caustic (70.8° to 72.7° depending on earthquake depth) traces with $P'P'bc$ STN ≥ 3.5 are saved and at greater distances seismograms with $P'P'df$ STN ≥ 3.0 are saved. A lower STN threshold is used for $P'P'df$ because of its smaller amplitude.

This automatic selection procedure identifies 1,218 seismograms meeting the minimum STN requirement. Visual inspection to discard records with data spikes or other problems produces a final data set of 1,089 seismograms.

To enhance the visibility of weak arrivals we stack the data. The *bc* branch of $P'P'$ is used as a reference phase for source–receiver ranges less than the *b* caustic and the *df* branch is used at greater ranges. All travel times are calculated using the *iasp*91 velocity model [*Kennett and Engdahl*, 1991]. The seismograms are stacked as follows:

High–frequency wavefield before $P'P'$

1) The source–receiver range is corrected to its zero depth equivalent by ray tracing from the hypocenter to the surface using the reference $P'P'$ ray parameter. Thus, stacked $P'P'$ arrivals with the same ray parameter will occupy the same distance bin.

2) The envelope function (positive outline) is calculated for each seismogram. This is done to avoid cancellation of incoherent arrivals when the data are stacked.

3) The average noise in a 40 s time window starting 200 s before the $P'P'$ arrival is subtracted from the envelope function and the trace is normalized to the maximum $P'P'$ amplitude. This accounts for varying signal and noise levels between traces. Shifting the start time of the noise window changes the DC offset of the stacked traces but does not significantly affect their shape.

4) Weights proportional to the STN of $P'P'$ are assigned to the traces. For this purpose, the STN is defined as the ratio of the maximum within a 20 s signal window starting at the $P'P'$ arrival time to the maximum taken in a 40 s noise window beginning 200 s before $P'P'$. Traces with STN greater than 10 are assigned a weight of 10. Processed traces from distances beyond the $P'P'$ *b* caustic having STN ≤ 2 and traces from distance ranges less than the *b* caustic having STN ≤ 4 are given a zero weight.

5) The processed seismograms are aligned on the predicted $P'P'$ onset, binned in range and time (3° × 6 s), and the weighted average is calculated and plotted.

Figure 2 shows the resulting stack of the high–frequency wavefield preceding $P'P'$, containing data from 994 seismograms (95 of the 1,089 traces were assigned zero weight during the stacking procedure). The stacked traces are normalized to the maximum $P'P'$ amplitude and are plotted with respect to the origin time of a zero depth earthquake. To aid in visualization, the thick traces are magnified by a factor of eight at distance ranges less than the $PKKP$ *c* caustic (72°) and for times prior to 55 s before $P'P'$. An ASCII data file of the stack can be obtained from *GRL online*.

Several documented high–frequency arrivals appear in the stacks. Figure 2B displays calculated travel–time curves for the observed phases. The travel–time curves for $P'P'$ (the small amplitude *cd* branch is not shown), mark the onset time of the largest arrival and the italic "*b*" indicates the position of the $P'P'$ *b* caustic near 71°. The detection of the small amplitude $P'_{660}P'$ arrival verifies the efficiency of the stacking

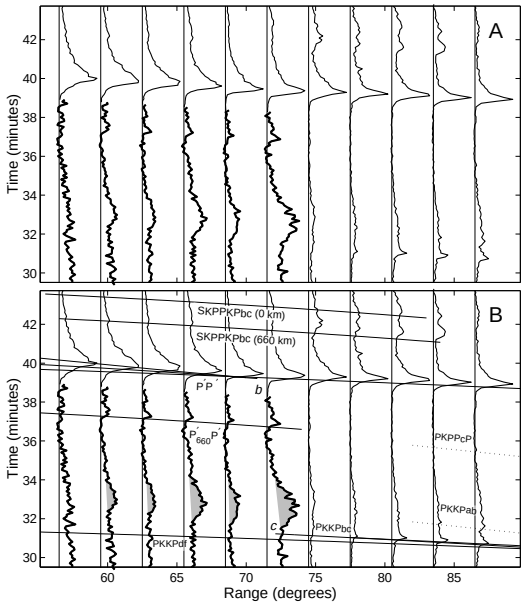

Figure 2. (A) Stack of 994 seismograms showing the high–frequency wavefie ld preceding $P'P'$. Note the broad emergent arrival, which we term $PKKP_X$, imaged between 59.5° and 71.5° (possibly to greater ranges) starting at ∼31.7 minutes. The stacked traces are normalized to the maximum $P'P'$ amplitude and are plotted with respect to the origin time of a zero depth earthquake. To better show the $PKKP_X$ arrival, amplitudes are magnified by 8 for traces preceding $P'P'$ at ranges less than 73° (indicated by the heavy lines). (B) Data stack with travel times of observed phases marked. Positions of the $P'P'$ *b* caustic and $PKKP$ *c* caustic are labeled with the italic *b* and *c* respectively and the $PKKP_X$ arrival is highlighted in gray.

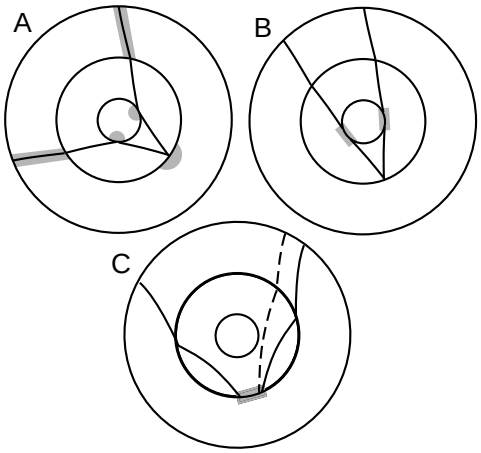

Figure 3. $PKKP$ ray paths with gray regions indicating possible places where scattering and/or diffraction may be occurring. A) Regions considered for single scattering. B) The ray geometry for ICB diffracted energy. $PKKP$ energy may be diffracted at either or both of the ICB interaction points. C) The ray geometry for CMB diffracted (solid line) and diffracted–scattered (dashed line) energy. $PKKP$ is shown diffracting and scattering at the core reflection point. However, $PKKP$ may diffract at any of the three CMB interaction points and can also scatter out of the plane of the page.

method. $P'_{660}P'$ energy travels a similar path to $P'P'$, but reflects off the underside of the 660–km discontinuity instead of the surface [*Engdahl and Flinn*, 1969].

Combining data from different depth earthquakes and aligning on the predicted $P'P'$ arrival time before stacking generates two peaks corresponding to the $SKPPKP$ arrival, a result of a change in $P'P'$–$SKPPKP$ differential travel time with earthquake depth and the bimodal seismicity depth distribution. The onset times of the two peaks roughly agree with the predicted $SKPPKP$ travel times for hypocenters at 0 km and 660 km (see Figure 2B).

The stack contains arrivals associated with the *ab* and *bc* branches of *PKKP*. An impulsive $PKKPbc$ arrival is observed to distances of 77.5°. $PKKPab$ energy is visible at ranges as short as 83.5°, far less than its ray theoretical limit of ∼105°, a result of energy tunneling along the CMB [*Engdahl*, 1968; *Richards*, 1973]. The small, gradual rise in energy preceding $PKKPbc$ at ranges beyond 77° may result from energy scattered from topography at the CMB [*Doornbos*, 1980; *Earle and Shearer*, 1997].

The broad emergent arrival imaged between 59.5° and 71.5° extending from the *PKKP c* caustic (indicated with gray shading in Figure 2B) to our knowledge is undocumented and will be referred to as $PKKP_X$. $PKKP_X$ is superimposed on the *S* and *SP* coda (the steady decrease in amplitude with increasing time seen in the thick magnified traces).

Several salient features characterize $PKKP_X$. Starting near the *PKKP c* caustic, the arrival has an emergent onset, a long duration (up to 150 s), and an amplitude that diminishes with decreasing distance. The long duration is not indicative of a low frequency arrival because the traces have been high–pass filtered before stacking. Instead, the envelope images an extended short–period wavetrain. The emergent onset and long duration can also be seen in stacks made from data restricted to shallow events (≤ 50 km); thus, these characteristics do not arise from combining data from different depths.

Before discussing the possible origin of $PKKP_X$, we mention several phases which are poorly imaged or not seen in Figure 2. Deep earthquakes produce $SKKKP$ arrivals which precede $P'P'$ by up to one minute. *SKKKP* is not seen in our stack due to its small amplitude and the depth dependent $P'P'$–$SKKKP$ travel time.

The small arrival seen near 86.5° and 35.3 minutes is the "wrap around" phase $PKPPcP$ arriving beyond its ray–theoretical limit of 90°. The predicted arrival time and moveout for $PKPPcP_{diff}$ are similar to $P'_{660}P'$ and in principle these two arrivals could be confused. However, the stack (Figure 2) does not continuously image $PKPPcP_{diff}$ between 74° and 84°, thus, we believe the phase seen between 59.5° and 74.5° at ∼37 minutes is $P'_{660}P'$ (Figure 2B). No consistent $P'_{410}P'$ arrival is observed, indicating that more high–frequency energy is reflected from the 660–km discontinuity than from the 410–km discontinuity. This observation agrees with previous studies in which observations of $P'_{660}P'$ are more common than $P'_{410}P'$ [e.g., *Benz and Vidale*, 1993]. As more data become available in the future, stacks with improved signal–to–noise will become possible and should be able to better address questions regarding the relative reflectivity of the 410– and 660–km discontinuities and the possible existence of smaller discontinuities.

Discussion

What is the origin of $PKKP_X$? A scattering source is indicated by its emergent onset and long duration, and it appears related to $PKKP$ given the start times and reduced amplitude with increased separation from the *PKKP c* caustic. If the energy originates as $PKKP$, it must be scattered from either the *ab* or *bc* branch to ranges shorter than the *c* caustic near 72° (scattering from the *df* branch seems unlikely since the direct *df* phase is not observed). Possible ways in which this could occur are illustrated in Figure 3. Scattering within the liquid outer core is unlikely, as there is no evidence for lateral velocity or density variations in the outer core. First considering single scattering models, the possible scattering source regions include the mantle, the CMB and the ICB (see gray regions Figure 3A). Single scattering in the mantle or at the $PKKP$ CMB entry or exit points is an attractive candidate since PKP precursor studies have indicated that small–scale velocity heterogeneity is present at the CMB and throughout much of the mantle [e.g., *Cleary and Haddon*, 1972; *Bataille and Flatte*, 1988; *Hedlin et al.*, 1997]. However, our preliminary calculations using Born scattering theory indicate that realistic levels of mantle heterogeneity predict arrivals with amplitudes at least ten times smaller than those observed. Scattering occurring at the ICB or at the CMB reflection point also cannot explain the observations, given that the minimum travel time for $PKKP$ energy single scattered from these regions precedes the observed onset of the arrival by more than one minute at 60°. Therefore, we do not find any single–scattering models that provide an adequate explanation for the observed arrivals and now discuss multiple–scattering models.

The *PKKP c* caustic marks the position where energy

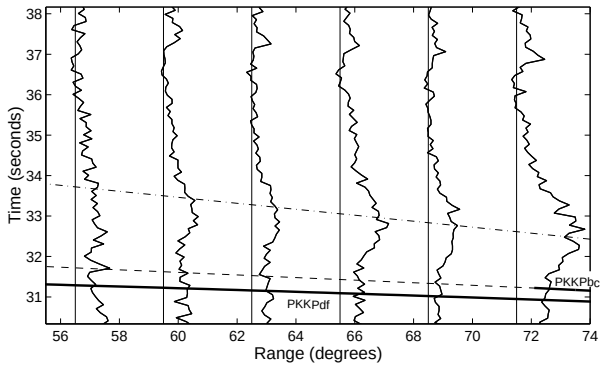

Figure 4. The $PKKP_X$ arrival with travel time predictions for ICB (dashed line) and CMB (dashed–dotted line) diffracted energy.

first encounters the inner core. Given the proximity of the arrival's apparent onset to this point, a mechanism involving diffraction or multiple scattering at the ICB seems plausible (see Figure 3B). In this case, $PKKP_X$ would be analogous to observations of high–frequency P_{diff} coda that have been interpreted as resulting from multiple scattering within a wave guide near the CMB [*Bataille and Lund*, 1996]. However, the moveout of $PKKP_X$ does not appear to closely match that predicted for energy propagating along the ICB (Figure 4). Although $PKKP_X$ seems to extend from the coda of $PKKPbc$, it may also be present at distances $> 72^\circ$ and linked in some way to the PKKPab branch, perhaps as a result of near–CMB scattering. A multiple–scattering model involving diffraction along the CMB was previously used to explain observations of an extended short–period P coda following P_{diff} [*Bataille and Lund*, 1996]. The model assumes a low–velocity heterogeneous zone just above the CMB. P energy is channeled into the low–velocity zone where it undergoes multiple scattering at small–scale heterogeneities and is continuously leaked into the mantle and core. Evidence for heterogenous low velocity zone above the CMB is seen in observations of anomalus SP_dKS arrivals [*Garnero and Helmberger*, 1996]. Figure 3C shows an example ray path for $PKKP$ diffracted energy (solid line) and for $PKKP$ diffracted–scattered energy (dashed line). Energy encountering and leaving the CMB region from all incidence angles can contribute to the scattered wavetrain. However, energy will most efficiently enter and exit at greater angles of incidence. The dashed–dotted line in Figure 4 shows the predicted onset time for the non–scattered CMB diffracted $PKKPab$ arrival. Clearly the predicted onset time is later than the $PKKP_X$ onset; however, given the maximum travel time nature of $PKKP$ with respect to perturbations of its reflection point on the CMB it is possible to obtain scattered energy preceding the diffracted arrival. Thus it is conceivable that this mechanism could explain the observations.

Rigorous testing of these different hypotheses will require synthetic calculations of the shape and amplitude of predicted scattering envelopes that are beyond the scope of this paper. However, $PKKP_X$ represents a significant unexplained feature of the high–frequency seismic wavefield. Determining its origin may lead to an improved understanding of the magnitude and distribution of small–scale scatterers within the Earth.

Acknowledgments. We thank IRIS and the GSN for providing the data and Ed Garnero for his review. This work was supported by NSF grant (EAR93–15060).

References

Astiz, L., P. Earle, and P. Shearer, Global stacking of broadband seismograms, *Seismo. Res. Lett., 67,* 8-18, 1996.

Bataille, K., and F. Lund, Strong scattering of short-period seismic waves by the core-mantle boundary and the P-diffracted wave, *Geophys. Res. Lett., 23,* 2413-2416, 1996.

Bataille, K., and S. M. Flatte, Inhomogeneities near the core-mantle boundary inferred from short-period scattered PKP waves recorded at the Global Digital Seismograph Network, *J. Geophys. Res., 93,* 15057-15064, 1988.

Benz, H. M., and J. E. Vidale, Sharpness of upper-mantle discontinuities determined from high-frequency reflections, *Nature, 365,* 147-150, 1993.

Chang, A. C., and J. R. Cleary, Precursors to PKKP, *Bull. Seismol. Soc. Am., 68,* 1059-1079, 1978.

Cleary, J. R., and R. A. W. Haddon, Seismic wave scattering near the core-mantle boundary: A new interpretation of precursors to PKP, *Nature, 240,* 549-551, 1972.

Doornbos, D. J., The effect of a rough core-mantle boundary on PKKP, *Phys. Earth Planet. Inter., 21,* 351-358, 1980.

Doornbos, D. J., Seismic wave scattering near caustics: Observations of PKKP precursors, *Nature, 247,* 352-353, 1974.

Engdahl, E. R., Seismic waves within Earth's outer core— Multiple reflection *Science, 161,* 263-264, 1968.

Engdahl, E. R., and E. A. Flinn, Seismic waves reflected from discontinuities within Earth's upper mantle, *Science, 163,* 177-179, 1969.

Earle, P. S., and P. M. Shearer, Observations of PKKP precursors used to estimate small–scale topography on the core–mantle boundary, *Science, 277,* 667-670, 1997.

Garnero, E. J. and D. V. Helmberger, Seismic detection of a thin laterally varying boundary layer at the base of the mantle beneath the Central–Pacific, *Geophys. Res. Lett., 23,* 977-980. 1996.

Hedlin, M. A., P. M. Shearer, and P. S. Earle, Seismic evidence for small-scale heterogeneity throughout the Earth's mantle, *Nature, 387,* 145-150, 1997.

Kennett, B. L. N., and E. R. Engdahl, Traveltimes for global earthquake location and phase identification, *Geophys. J. Int., 105,* 429-465, 1991.

Lay, T., and T.C. Wallace, *Modern Global Seismology,* 521 pp., Academic Press, Inc., London, 1995.

Richards, P. G., Calculation of body waves, for caustics and tunnelling in core phases, *Geophys. J. R. Astron. Soc., 35,* 243-264, 1973.

Vidale, J. E., and H. M. Benz, A sharp and flat section of the core-mantle boundary, *Nature, 359,* 627-629, 1992.

P. S. Earle, and P. M. Shearer, SIO-0225, Scripps Institution of Oceanography, University of California, San Diego, La Jolla, CA 92093-0225

(Received June 27, 1997; revised October 29, 1997; accepted November 17, 1997.)